Passively Q-Switched Dual-Wavelength Laser Operation With Coaxially End-Pumped Composite Laser Materials

Xianzhong Zhang, Kai Zhong, Hongzhan Qiao, Fangjie Li, Yizhe Zheng, Degang Xu, and Jianquan Yao

***Abstract*—A passively Q-switched dual-wavelength laser with tunable power ratio and pulse interval is demonstrated based on the coaxial diode end-pumping configuration by varying the pump wavelength. A theoretical model was built by a set of time-domain rate equations illustrating the dynamic process of both the pulse generation of two wavelengths from a shared pump source and a saturable absorber. The simulation showed that both the power ratio and the time interval between the pulses at two resonant wavelengths in the Q-switched mode could be tuned by balancing the gains in two laser crystals by varying the pump wavelength, realized by controlling the working temperature of the pump laser diode. The experiment was performed with Nd:YAG/Nd:YAP composite laser crystals and a Cr^{4+}:YAG slice working as the saturable absorber for pulse generation. The continuous-wave and Q-switched total output power reached 5.62 W and 2.12 W, corresponding to overall optical-optical conversion efficiencies of 37.5% and 14.1%, respectively. The manipulation of power ratio and pulse interval between 1064 nm and 1080 nm agreed well with the simulation results.**

***Index Terms*—Coaxially diode end-pumping, dual-wavelength laser, passively Q-switching.**

I. Introduction

PULSED dual-wavelength lasers are of great interest in applications such as terahertz generation, remote sensing, precision measurement, and spectroscopy [1]–[4]. Conventional methods to realize simultaneous dual-wavelength laser operation depend on gain balancing of two oscillating wavelengths originating from transitions between different energy levels or Stark sublevels of the laser gain medium, such as Nd:YAG, Nd:YLF and Nd:YAP [5]–[7]. Given the material has a broad gain bandwidth, e.g., Ti:sapphire, alexandrite and Tm/Ho:YLF, inserting mode-selection elements into the cavity is effective in wavelength tuning and linewidth narrowing [8]–[10]. It's even more straightforward for fiber lasers to use fiber-coupled comb filters which generate wavelength-dependent fringes for dual-wavelength selection [11], [12]. The critical issue for the above approaches is balancing the gains between the resonant wavelengths from mode competition, thus the stability is delicate and sensitive to the working condition. Adopting two independent gain media has been proved feasible to eliminate mode competition at the expense of a more complex cavity and additional pump sources [13]–[15].

Recently, a laser diode (LD) end-pumping configuration with coaxial arranged two laser crystals was proposed for dual-wavelength laser generation [16]. It intrinsically eliminates gain competition and provides the possibility to tune the power ratio without any extra elements. A commonly used approach is varying the pump absorption and laser gain of each crystal by changing the pump focusing position [17]. To improve the laser stability, the pump absorption can also be adjusted by varying the temperature-dependent pump wavelength, which requires no mechanical change to the cavity [18], [19]. The pulse interval between two wavelengths was also controllable in the Q-switched regime, leading to the implementation of diverse nonlinear frequency converters [20]–[22]. It is believed that coaxially end-pumping is the most simple and compact scheme for flexible dual-wavelength lasers till now, and a step further to reduce the size and cost can be introducing passively Q-switching, which is really complicated including two laser crystals sharing the same pump and saturable absorber (SA).

In this paper, a theoretical model was built to simulate the dynamic process of a passively Q-switched dual-wavelength laser in the coaxially end-pumping configuration. The pump absorption and population inversion in each laser crystal, the ground-state population density of the SA and the photon density in the cavity at each wavelength were considered. The experiment was carried out with a Nd:YAG crystal and a Nd:YAP crystal to generate laser wavelengths at 1064 nm and 1080 nm, while a Cr^{4+}:YAG crystal was used as SA for Q-switching. The continuous-wave (CW) and Q-switched total output power reached 5.62 W and 2.12 W, respectively, under the LD pump power of 15 W, corresponding to the overall optical-optical conversion efficiencies of 37.5% and 14.1%. By varying the pump wavelength to change the gains in two laser crystals, the power ratio between two laser wavelengths could be tuned

Manuscript received August 31, 2021; revised October 5, 2021; accepted October 9, 2021. Date of publication October 14, 2021; date of current version October 27, 2021. This work was supported in part by the National Natural Science Foundation of China under Grant 61675146 and in part by the Natural Science Foundation of Tianjin City under Grant 18JCYBJC16700. *(Corresponding author: Kai Zhong.)*

The authors are with the School of Precision Instruments and Optoelectronics Engineering, Tianjin University, Tianjin 300072, China, and also with the Key Laboratory of Optoelectronics Information Technology (Ministry of Education), Tianjin University, Tianjin 300072, China (e-mail: zxzhitr@163.com; zhongkai1984@gmail.com; qiaohongzhan@hotmail.com; fangjie_lee@163.com; zhengyizhe_tju@163.com; xudegang@tju.edu.cn; jqyao@tju.edu.cn).

Digital Object Identifier 10.1109/JPHOT.2021.3120000

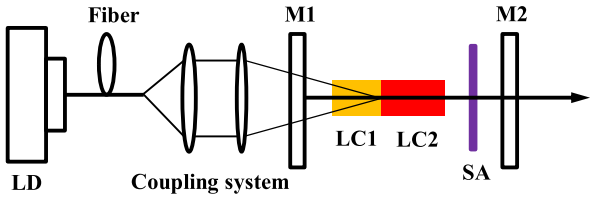

Fig. 1. Experimental layout of a coaxial diode-end-pumped passively Q-switched dual-wavelength laser.

and their pulse interval was also adjustable in the Q-switched mode.

II. Theoretical Mode and Numerical Analysis

The diagram for a LD coaxially end-pumped passively Q-switched dual-wavelength laser is shown in Fig. 1. The gain media is made up of two separate Nd^{3+} doped laser crystals (LC1 and LC2) with different host materials and an air gap of around 0.2 mm in between. The absorption peaks of LC1 and LC2 are slightly different, which provides an approach to change the pump absorption in each of the coaxially arranged crystals by tuning the temperature-dependent LD wavelength, so as to control the laser gain and the output power at each wavelength to realize tunable power ratio and pulse interval. All the end faces of two crystals are antireflection (AR) coated at the pump and resonant laser wavelengths. The cavity mirror M1 is AR for the pump beam and high reflection (HR) at two laser wavelengths, while M2 has partial laser transmission for outcoupling. An SA (Cr^{4+}:YAG crystal) with AR coatings at two laser wavelengths at both end faces was used as the passive Q-switch for pulse generation.

Based on the theoretical model we put forward for the coaxial diode end-pumping configuration [19], the CW output power at each wavelength is given by

$$P_{out,i} = \frac{1}{2} A_i \left(1 - R_i\right) I_{s,i} \left(\frac{2 g_{0,i} l_i}{\delta_i} - 1\right) \tag{1}$$

where the subscript i (1 or 2) denotes the physical quantity relating to different laser crystals (LC1 or LC2). A is the effective laser beam cross section, R is the reflectivity of the output mirror, I_s is the saturation power density, l is the crystal length, g_0 is the small-signal gain and δ is the remaining round-trip dissipative laser loss originating from reflection, absorption and diffraction, etc.

The coupled rate equations for a four-level laser system are used to model a passively Q-switched laser [23]. It's noticeable that in coaxial end-pumping two laser crystals are pumped by the same LD and share the same SA, but the dynamic process of pulse building and releasing for each wavelength is independent. On this basis, the rate equations of the coaxially end-pumped passively Q-switched dual-wavelength laser can be obtained by introducing the population inversion and intracavity photon density generated in each laser crystal, expressed as

$$\frac{d\phi_i}{dt} = \frac{\phi_i}{t_r} \left[2\sigma_i n_i l_i – 2\sigma_{gs} n_{gs} l_s - 2\sigma_{es}\left(n_{0s} - n_{gs}\right) l_s - \left(\ln\frac{1}{R_i} + \delta_i\right)\right] \tag{2}$$

$$\frac{dn_i}{dt} = R_{pi}\left(N_i - n_i\right) - \gamma \sigma_i \nu_i \phi_i n_i - \frac{n_i}{\tau_{ai}} \tag{3}$$

$$\frac{dn_{gs}}{dt} = \frac{n_{0s} - n_{gs}}{\tau_{gs}} - \sigma_{gs} c \phi_{sum} n_{gs} \tag{4}$$

In (2), ϕ is the intracavity photon density, $tr = 2l'/c$ is the round-trip transit time of light in the cavity optical length l', c is the light speed in vacuum. σ is the stimulated emission cross section, n is the inverted population density, n_{0s} is the ground-state population density of SA, l is the crystal length, σ_{gs} and σ_{es} are ground- and excited-state absorption cross sections of the SA, respectively, and l_s is the SA length. n_{0s} is the total population densities of SA, given by

$$n_{0s} = -\frac{\ln T_0}{\sigma_{gs} l_s} \tag{5}$$

where T_0 is the initial transmission of the SA.

In (3), N is the total active ions density of laser crystal, γ is the inversion reduction factor ($\gamma = 1$ and $\gamma = 2$ correspond to four-level and three-level systems, respectively), ν is the light velocity in the laser crystal, and τ_a is the upper-laser-level lifetime of the laser gain medium. R_p is the pump coefficient related to the absorbed pump power in each crystal, written as an integral form

$$R_{pi} = \frac{\eta_i p_i \alpha_i}{N_i h \nu_p l_i} \int \frac{e^{-\alpha_i z}}{\pi w_p^2(z)} dz \tag{6}$$

in which η is the quantum efficiency, p is the incident pump power at the crystal entrance face, N is the number of total active ions, α is the wavelength-dependent absorption coefficient, ν_p is the pump frequency, $w_p(z)$ is the pump beam radius along the propagation direction, which is related to the beam waist w_0 and the waist location z_0, and $z = 0$ indicates at the boundary of two crystals.

In (4), τ_{gs} is the ground state recovery time of the SA and $\phi_{sum} = \phi_1 + \phi_2$ is the sum of photon densities originated from two laser crystals considering that the photons at both laser wavelengths contribute to the bleaching of the SA.

For the case that LC1 is a 7-mm-long 0.4-at%-doped Nd:YAG crystal and LC2 is a 8-mm-long, 0.9-at%-doped b-cut Nd:YAP crystal, the CW output power and pulse characteristics versus LD wavelength (or temperature) can be calculated from (1)–(5). The crystals were selected because they have close but different absorption peaks, which were 805 nm and 804 nm for the Nd:YAG and Nd:YAP crystals, respectively, from the experimental characterization shown in Fig. 2(a). If their relative positions are inverted, the Nd:YAG laser can not oscillate since little pump power is left after passing the Nd:YAP crystal which has a larger size and higher absorption coefficient. A 50-W LD (NL-P4-50-0808-3) with the pump wavelength at around 800 nm was used as the pump source. The LD pump beam was coupled by an optical fiber with the numerical aperture of 0.22 and core diameter of 400 μm, and then focused by a 1:1 coupling system into the gain media. The SA had an initial transmission of $T_0 =$

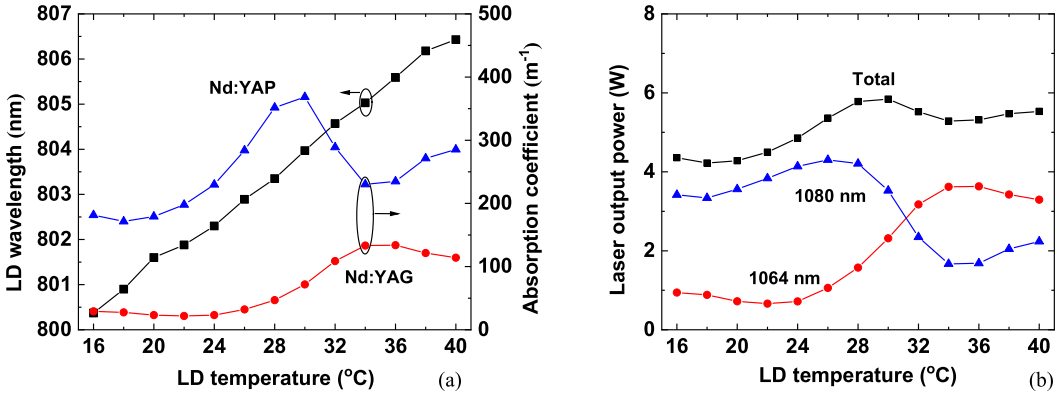

Fig. 2. (a) Experimental characterization of the temperature-dependent LD wavelength and absorption coefficients in the Nd:YAG and Nd:YAP crystals and (b) the theoretical output powers of the CW dual-wavelength laser in total and at each wavelength.

80%. The remaining parameters used in simulations are: $z_0 = -1$ mm, $w_0 = 200$ μm, $M^2 = 50$, $n_1 = 1.94$, $n_2 = 1.82$, $p = 15$ W, $l_1 = 7$ mm, $l_2 = 8$ mm, $N_1 = 0.56\times10^{26}$ m^{-3}, $N_2 = 1.26 \times 10^{26}$ m^{-3}, $\tau_1 = 230$ μs, $\tau_2 = 170$ μs, $\sigma_1 = 2.8\times10^{-23}$ m^{-2}, $\sigma_2 = 2.2 \times 10^{-23}$ m^{-2}, $\sigma_{gs} = 8.7 \times 10^{-23}$ m^{-2}, $\sigma_{es} = 2.2 \times 10^{-23}$ m^{-2}, $l_s = 1$ mm, $\tau_{gs} = 3$ μs, and $T = 10\%$.

Firstly, we simulated the output power of the CW dual-wavelength laser without the SA, pumping at different LD wavelengths. The theoretical results are shown in Fig. 2(b). A total power of 5.84 W is generated when the LD temperature is 30 °C (LD wavelength: 804 nm) and the overall conversion efficiency is 38.9%. Benefitting from the significant difference in the absorption spectra of Nd:YAG and Nd:YAP given in Fig. 2(a), the power ratio between 1064 and 1080 nm is continuously tunable from 0.17 to 2.17, covering a much wider range than that of [19] in which two laser crystals have similar absorption spectra.

For Q-switched operation, the inverted population density of two laser crystals (from Fig. 3(a) to Fig. 3(c)), ground-state population density of the SA (from Fig. 3(d) to Fig. 3(f)) and intracavity photon density at two laser wavelengths (from Fig. 3(g) to Fig. 3(i)) were simulated simultaneously, as three physical quantities are coupled and interactive. Two crystals and the related lasing wavelengths are also connected by sharing the same pump source and Q-switch. The temporal details of the laser pulses picked from the pulse trains is shown from Fig. 3(j) to Fig. 3(l). The pump wavelengths in consideration include 803.4 nm (28 °C), 804 nm (30 °C) and 804.6 nm (32 °C), corresponding to different pulse sequence orders at laser wavelengths of 1064 nm and 1080 nm. Clearly, the pulse building process for each wavelength relies on the accumulated population inversion. Therefore, varying the LD temperature (wavelength) changes the pump absorption in each crystal and affects the temporal pulse dynamic process. The pulses at two wavelengths are synchronized when the LD temperature is 30 °C and their interval is tunable to facilitate different applications. It should also be noted that the pulse repetition rate is not constant, for example, the pulse repetition rates are 13.2 kHz, 10.9 kHz and 15.3 kHz when the LD operates at 28 °C, 30 °C and 32 °C, respectively. If the LD wavelength favors one of the laser crystals to establish preponderance in population inversion (e.g., Fig. 3(a) and Fig. 3(c)), the resultant strong spontaneous emission would quickly bleach the SA and trigger two laser pulses. The lowest repetition rate should occur when two pulses are near synchronization, shown in Fig. 3(b).

III. Experimental Results and Discusion

The output characteristics for the CW coaxially end-pumped dual-wavelength Nd:YAG/NdYAP laser at 1064 nm and 1080 nm were measured by removing the SA in Fig. 1. The LD temperature was tuned to be 31 °C (804.2 nm) and the pump focusing position was at $z = -1$ mm, in order to balance the gains in two laser crystals at the maximum incident pump power of 15 W. By using a band-pass filter at 1064 nm (Thorlabs FL1064-3), two beams were separated to measure their individual output powers. The CW output powers at each laser wavelength and the total versus the incident pump power are shown in Fig. 4(a). The total output power increased almost linearly with the pump power and reached 5.24 W when the incident pump power was 15 W, corresponding to the overall optical-optical conversion efficiency of 34.9%. The output powers were 2.63 W at 1064 nm and 2.61 W at 1080 nm, almost equivalent to each other.

As a validation of the simulation results in Fig. 2(b), the output power of the dual-wavelength laser was also measured at different LD temperatures (wavelengths) with the same incident pump power of 15 W. As shown in Fig. 4(b), the power ratio between 1064 nm and 1080 nm could be tuned from 0.19 (24 °C, 802.3 nm) to 2.95 (34 °C, 805 nm). The significant change of the power ratio from 28 °C to 34 °C was caused by the difference in absorption spectra between two laser crystals. The maximum total CW output power of 5.62 W (1.49 W at 1064 nm and 4.13 W at 1080 nm) was obtained when the LD was operating at 28 °C (803.4 nm), corresponding to the conversion efficiency of 37.5%, which agreed well with the theoretical results. The total output power slightly decreased if the LD worked at higher temperature than 34 °C. The reason of the departure from Fig. 2(b) was that the actual LD output power slightly declines with the increase of wavelength, whereas it was assumed to be constant in simulation. The output spectrum of the dual-wavelength laser was

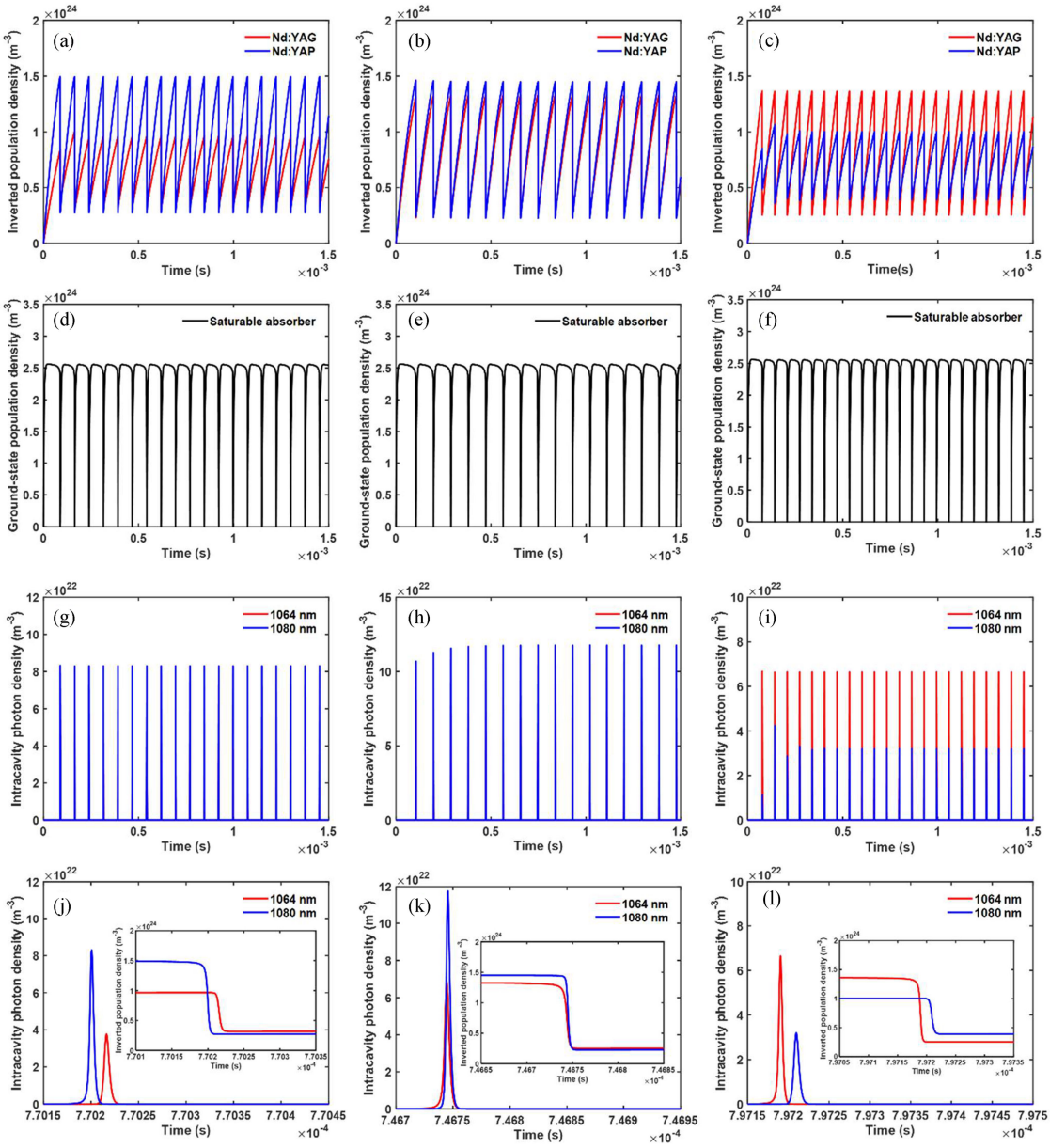

Fig. 3. Simulation of the dynamics of a coaxial end-pumped passively Q-switched dual-wavelength Nd:YAG/Nd:YAP laser. (a)–(c): inverted population density of two laser crystals; (d)–(f): ground-state population density of SA; (g)–(i): pulse train of the intracavity photon density at two laser wavelengths; (j)–(l): details of the temporal pulses, and the inset depicts the population inversion of the corresponding pulse. (a), (d), (g), and (j) are calculated at LD temperature of 28 °C (803.4 nm), (b), (e), (h), and (k) are at 30 °C (804 nm), and (c), (f), (i), and (l) are at 32 °C (804.57 nm).

monitored with an Agilent 86142B optical spectrum analyzer and typical examples are given in Fig. 5. Three figures were recorded at different LD temperatures of 26 °C (802.9 nm), 31 °C (804.2 nm) and 36 °C (805.6 nm), respectively, intuitively indicating the power ratio between 1064 nm and 1080 nm could be effectively adjusted.

Provided that the SA was inserted into the cavity, the output power characteristics of the passively Q-switched dual-wavelength Nd:YAG/Nd:YAP laser were measured. Fig. 6(a) gives the output power versus pump power when the LD temperature was 31 °C (804.2 nm) and the pump focusing position of $z = -1$ mm was unchanged. The total output power in the Q-switching mode reached 1.5 W, in which they were 0.72 W and 0.78 W at 1064 nm and 1080 nm, respectively, with the overall slope efficiency of 14.4%. The dramatic power decline compared with that of CW operation was mainly caused by the insertion loss of SA and the inevitable spontaneous emission between two adjacent laser pulses. The power ratio between 1064 nm and 1080 nm is shown in Fig. 6(b), which was continuously tunable from 0.07 to 7.56. The maximum total output power was 2.12 W (0.15 W at 1064 nm and 1.97 W at 1080 nm) when the LD operated at 24 °C (802.3 nm) and the incident pump power was 15 W, corresponding to the slope efficiency of 20.4%. The total output power went down faster than that of the CW mode in the 28–34 °C temperature range because of the insertion loss of the SA, which would introduce more

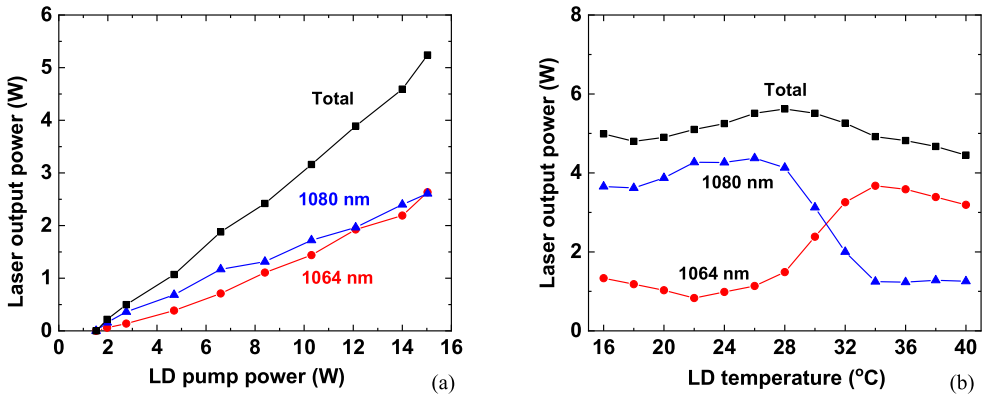

Fig. 4. Experimental output power of the CW coaxially end-pumped dual-wavelength Nd:YAG/NdYAP laser. (a) output power versus incident pump power; (b) output powers at each wavelength and the total versus LD temperature (pump wavelength) when the pump power was 15 W.

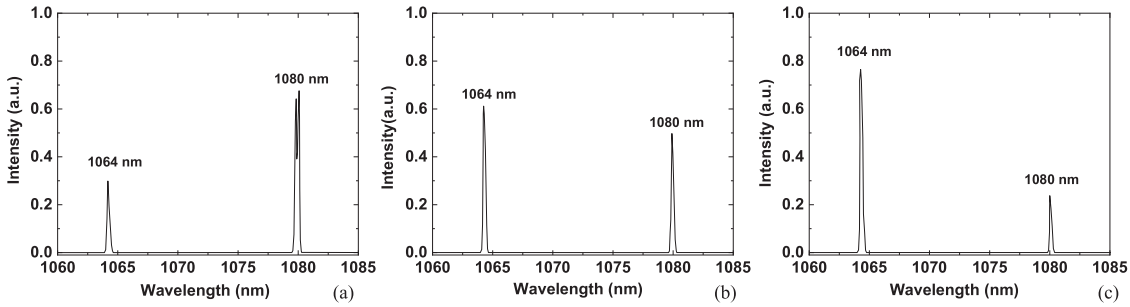

Fig. 5. Typical output spectra of the CW coaxially end-pumped dual-wavelength Nd:YAG/Nd:YAP laser when the pump power was 15 W. (a) LD temperature at 26 °C (802.9 nm); (b) LD temperature at 31 °C (804.2 nm); (c) LD temperature at 36 °C (805.6 nm).

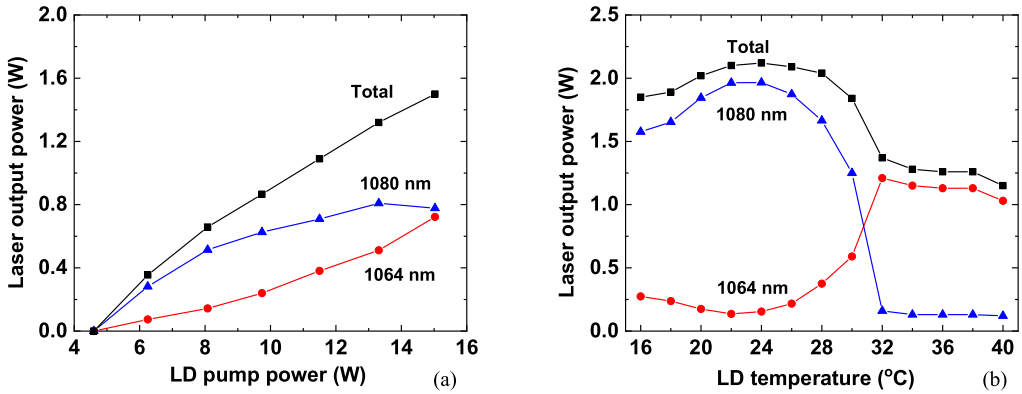

Fig. 6. Output power characteristics of the coaxially end-pumped passively Q-switched dual-wavelength Nd:YAG/Nd:YAP laser. (a) laser output power versus incident LD pump power; (b) laser output power versus LD temperature when the incident pump power was 15 W.

depression to the underprivileged resonant wavelength, and for the same reason a larger power-ratio tuning range could be realized for the Q-switched operation. The output power stability was also investigated, shown in Fig. 7(a). The root mean square (RMS) instability during an hour was 1.42% for the total output power, and they were 2.03% and 2.75% at 1064 nm and 1080 nm, respectively. The beam quality factor (M^2) of the dual-wavelength laser was around 2 in both the horizontal (x) and vertical (y) directions, measured by the knife-edge method and shown in Fig. 7(b). The beam profile of the pure 1064 nm laser was also measured with the help of a bandpass filter, but there was little difference. Besides the nature that both laser wavelengths come from the same cavity, the other reason is that the unpolarized 1064 nm laser beam can be degraded when passing the birefringent Nd:YAP crystal, thus the M^2 factor is mainly restricted by the 1064 nm laser.

The temporal behavior of the dual-wavelength Nd:YAG/Nd:YAP laser at different LD temperatures

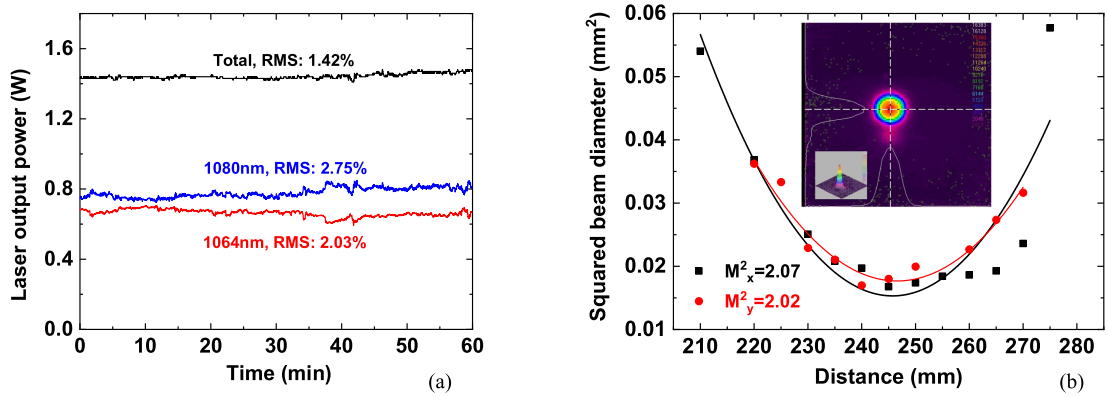

Fig. 7. Output power stability (a) and beam quality (b) of the coaxially end-pumped passively Q-switched dual-wavelength Nd:YAG/Nd:YAP laser. The LD temperature was 31 °C (804.2 nm) and the incident pump power was 15 W. The inset of (b) is the beam profile measured with a Spiricon Pyrocam III camera.

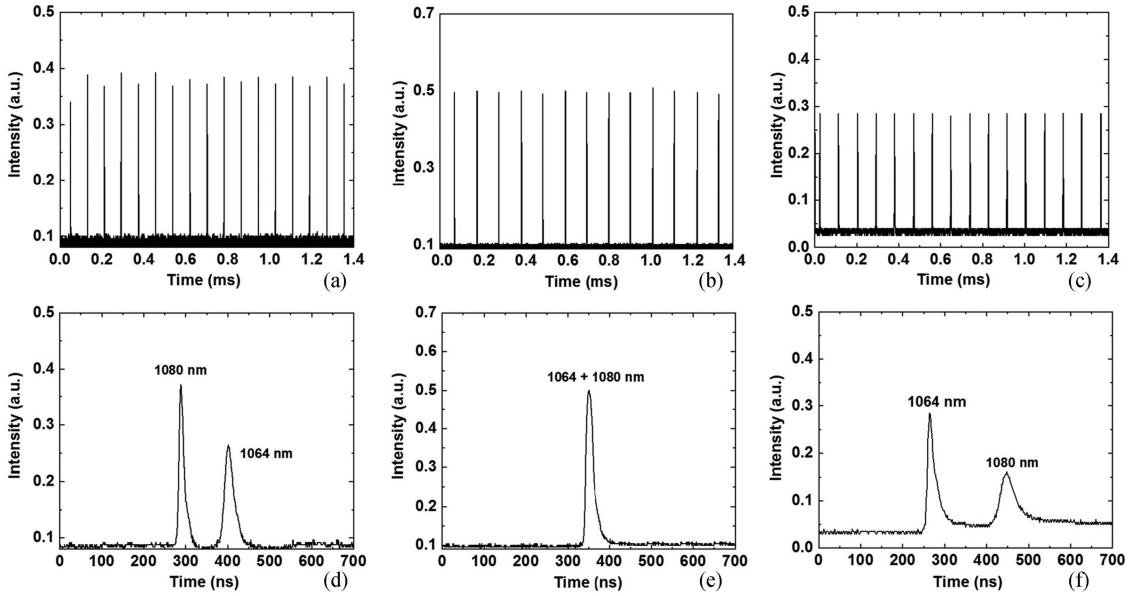

Fig. 8. Experimental results of the temporal pulse trains and detailed profiles of the coaxially end-pumped passively Q-switched dual-wavelength Nd:YAG/Nd:YAP laser when the pump power was 15 W. (a) and (d) are LD temperature at 28 °C (803.4 nm); (b) and (e) are LD temperature at 30 °C (804 nm); (c) and (f) are LD temperature at 32 °C (804.6 nm).

(wavelengths) was recorded by a fast-response InGaAs detector (Thorlabs DET08C), shown in Fig. 8. The pulse trains were quite stable as there was no competition between two laser wavelengths. In other words, two laser wavelengths inherently have no interactions after the saturable absorber is bleached, thus their pulse building and outputting process are totally independent. The pulse repetition rates were 12.3 kHz, 9.3 kHz and 11.6 kHz when the LD temperature was 28 °C (803.4 nm), 30 °C (804 nm) and 32 °C (804.6 nm), respectively. Basically, the results agreed well with the simulation, that is, the closer to the pulse synchronization condition, the lower repetition rates. The pulse width at 1064 nm declined if the LD temperature was increased from 28 °C (803.4 nm) to 32 °C (804.6 nm) while it was opposite at 1080 nm, which were in good accordance with the theoretical results. The reason is that the laser gain in Nd:YAG gradually grows with LD temperature within this range, leading to a shorter pulse building process. The synchronized pulse energies at 1064 nm and 1080 nm were 135 μJ and 63.7 μJ while the pulse widths were both around 19.6 ns, corresponding to the peak powers of 6.89 kW and 3.25 kW, respectively. The interval between two pulses could be roughly tuned from -110 ns to $+180$ ns, which could be used in the fields of pump-probing, differential optical absorption spectroscopy and nonlinear frequency conversion (e.g., terahertz wave generation).

IV. Conclusion

The characteristics of a coaxially end-pumped passively Q-switched dual-wavelength laser were studied both in theory and experiment. A theoretical model was built to analyze the output power and pulse generation process at two wavelengths from a

shared pump source and SA, and the simulation was performed based on coaxially arranged Nd:YAG/Nd:YAP laser crystals. The temporal behaviors of the inverted population density of two laser crystals, the ground-state population density of SA and the pulse-train generating process at two laser wavelengths not only revealed the dynamics of such a dual-wavelength laser, but also provided the approach to manipulate the pulse intervals between two wavelengths besides the average power ratio. The experimental results strongly supported the theoretical results. The power ratio between 1064 nm and 1080 nm was continuously tunable from 0.19 to 2.95 for CW operation and from 0.07 to 7.56 for the Q-switched mode. The pulse intervals could be adjusted within hundreds of nanoseconds. It is believed this is the most compact and robust method for flexible dual-wavelength laser generation, which has good prospects in various application areas.

REFERENCES

[1] K. Zhong *et al.*, "Optically pumped terahertz sources," *Sci. China Technol. Sci.*, vol. 60, no. 12, pp. 1801–1818, Jun. 2017.

[2] H. N. Y. Nguyen and W. Steenbergen, "Feasibility of identifying reflection artifacts in photoacoustic imaging using two-wavelength excitation," *Biomed. Opt. Exp.*, vol. 11, no. 10, pp. 5745–5759, Oct. 2020.

[3] M. Aoki and H. Iwai, "Dual-wavelength locking technique for coherent 2-μm differential absorption lidar applications," *Appl. Opt.*, vol. 60, no. 14, pp. 4259–4265, May 2021.

[4] Y. Wang *et al.*, "Study of signal enhancement in collinear femtosecond-nanosecond double-pulse laser-induced breakdown spectroscopy," *Opt. Laser Technol.*, vol. 122, 2019, Art. no. 105887.

[5] H. Lin, W. Zhu, R. Mu, H. Zhang, and F. Xiong, "Q-switched dual-wavelength laser at 1116 and 1123 nm using WS 2 saturable absorber," *IEEE Photon. Tech. Lett.*, vol. 30, no. 3, pp. 285–288, Feb. 2018.

[6] Z. Tu *et al.*, "Efficient high-power orthogonally-polarized dual-wavelength Nd:YLF laser at 1314 and 1321 nm," *Opt. Exp.*, vol. 27, no. 23, pp. 32949–32957, Nov. 2019.

[7] W. Nie *et al.*, "Dual-wavelength waveguide lasers at 1064 and 1079 nm in Nd:YAP crystal by direct femtosecond laser writing," *Opt. Lett.*, vol. 40, no. 10, pp. 2437–2440, May 2015.

[8] G. Shayeganrad, "Tunable single-and dual-wavelength nanosecond Ti: Sapphire laser around 765 nm," *Appl. Phys. B*, vol. 124, no. 8, pp. 1–6, Jul. 2018.

[9] S. Ghanbari and A. Major, "High power continuous-wave dual-wavelength alexandrite laser," *Laser Phys. Lett.*, vol. 14, no. 10, Sep. 2017, Art. no. 105001.

[10] X. Zhang, T. Guo, P. Kang, and J. Huang, "Compact dual-crystal Tm, Ho: YLF laser with balanced orthogonal polarization output power," *Opt. Exp.*, vol. 29, no. 16, pp. 25762–25770, Aug. 2021.

[11] B. Ibarra-Escamilla *et al.*, "Dual-wavelength thulium-doped fiber laser with separate wavelengths selection based on a two mmi filters configuration," *Laser Phys.*, vol. 28, no. 9, Jul. 2018, Art. no. 095107.

[12] N. M. Yusoff, L. K. Yao, A. H. Sulaiman, N. M. Yusoff, and M. A. Mahdi, "Stable dual-wavelength laser incorporating polarization-maintaining erbium-doped fiber," *Opt. Laser Technol.,* vol. 135, 2021, Art. no. 106707.

[13] J. Sun, C. Zeng, Y. Dong, C. Wu, and G. Jin, "Electro-optic Q-switched dual-wavelength coaxial alternating output laser at 1064 and 1319 nm," *Infrared Phys. Technol.*, vol. 108, 2020, Art. no. 103354.

[14] Y. Zhang *et al.*, "Experimental investigation on the Y-type cavity tunable dual-wavelength laser based on neodymium-doped vanadate crystals," *Opt. Commun.*, vol. 495, 2021, Art. no. 127089.

[15] S. Men, Z. Liu, Z. Conga, Y. Li, and X. Zhang, "Electro-optically Q-switched dual-wavelength Nd: YLF laser emitting at 1047 nm and 1053 nm," *Opt. Laser Technol.,* vol. 68, pp. 48–51, Nov. 2014.

[16] Y. Liu *et al.*, "Compact and flexible dual-wavelength laser generation in coaxial diode-end-pumped configuration," *IEEE Photon. J.*, vol. 9, no. 1, Feb. 2017, Art. no. 1500210.

[17] H. Liang, T. Huang, F. Chang, C. Sung, and Y. Chen, "Flexibly controlling the power ratio of dual-wavelength SESAM-based mode-locked lasers with wedged-bonded Nd:YVO_4/Nd:$GdVO_4$ crystals," *IEEE J. Sel. Top. Quantum Electron.*, vol. 24, no. 5, pp. 1–5, Sep. 2018.

[18] M. Nadimi, C. Onyenekwu, and A. Major, "Continuous-wave dual-wavelength operation of the in-band diode-pumped Nd:$GdVO_4$/Nd:YVO_4 composite laser with controllable spectral power ratio," *Appl. Phys. B*, vol. 126, no. 5, pp. 1–5, Apr. 2020.

[19] X. Zhang *et al.*, "Theory and experiments of a power-ratio tunable dual-wavelength Nd:YVO_4/Nd:$GdVO_4$ laser by varying the pump wavelength," *Opt. Eng.*, vol. 60, no. 8, Aug. 2021, Art. no. 086103.

[20] Y. Liu *et al.*, "Compact and stable high-repetition-rate terahertz generation based on an efficient coaxially pumped dual-wavelength laser," *Opt. Exp.*, vol. 25, no. 25, pp. 31988–31996, Dec. 2017.

[21] Y. Liu *et al.*, "Dual-signal-resonant optical parametric oscillator intracavity driven by a coaxially end-pumped laser with compound gain media," *Opt. Exp.*, vol. 26, no. 16, pp. 20768–20776, Aug. 2018.

[22] Y. Liu *et al.*, "Dual-wavelength intracavity Raman laser driven by a coaxially pumped dual-crystal fundamental laser," *Opt. Exp.*, vol. 27, no. 20, pp. 27797–27806, Sep. 2019.

[23] X. Zhang, S. Zhao, Q. Wang, and Q. Zhang, "Optimization of Cr^{4+}-doped saturable-absorber Q-switched lasers," *IEEE J. Quantum Electron.*, vol. 33, no. 12, pp. 2286–2294, Dec. 1997.